Abrasive jet drilling of hard alumina flat: an experimental investigation and predictive modeling by ANN

Deb Kumar Adak[1,2], Prosenjit Dutta[2], Barun Haldar[3], Santanu Das[2*], Naser Abdulrahman Alsaleh[3], Sibsankar Dasmahapatra[2]

[1]*College of Engineering and Management, Kolaghat, Purba Medinipur, West Bengal, India*
[2]*Kalyani Government Engineering College, Kalyani, West Bengal, India*
[3]*College of Engineering, Imam Mohammad Ibn Saud Islamic University (IMSIU), Riyadh, Kingdom of Saudi Arabia*

KEYWORDS

Abrasive Jet Machining (AJM),
Alumina,
Drilling,
ANN,
Estimation.

ABSTRACT

Abrasive jet machining (AJM) is often applied in drilling of hard and brittle ceramic materials, and is also used for other processes like surface preparation, deburring, shot-peening, polishing, etc. AJM process parameters need be appropriately selected to have optimized responses like MRR, nozzle wear, etc. Experimental investigation is performed in this work by precisely controlling abrasive flow rate. Along with system pressure, abrasive flow rate, stand-off distance (SOD) and grain size are considered during performing AJM with silicon carbide abrasive on commercially pure 4 mm thick alumina tiles using response surface methodology (RSM). Analysis of variance is done to detect the relative significance of each of the variables. Artificial neural network (ANN) is constructed to estimate the response in AJM based on input parameters. Estimation of machining performance is effectively carried out by ANN based on the training data with less than 8% estimation error, particularly for MRR and NWR.

1. Introduction

The growing applications of ceramics, super alloys, composite materials and nanomaterials in the automotive, aerospace, medical and electronics industries are triggering challenges to machining industries. In this concern, abrasive erosion for machining difficult-to-machine materials are getting more important due to their efficient material removal capability which is more economical than big chip removal processes (Mattison, 1964). Although the history of development of abrasive technology like grinding started from circa 2000 B.C. in Egypt (Inasaki et al., 1993), abrasive machining technologies play a big role in manufacturing industries today due to typical favorable mechanical characteristics of abrasives, like hardness, heat resistance, toughness, friability (Linken, 2015), etc. Beyond grinding, different other abrasive material processing techniques are also being employed widely in industries at present (Kalpakjian & Schmid, 2007).

In the AJM process, materials are removed from the workpiece by a jet of air and abrasive mixture possessing high kinetic energy through erosion (Chauhan et al., 2008). The abrasive jet system came to the main-stream of commercial applications for cleaning and cutting just after introducing ceramic nozzle in the 1970s (Melentiev & Fang, 2018). This method is extensively used to drill hard and brittle materials (Liu et al., 2019). A similar abrasive jet formed by water is called abrasive water jet (Aydin et al., 2011), which is popular in industries for high-speed cutting of thin sheets to thick metal flat.

*Corresponding author,
E-mail: sdas.me@gmail.com

1.1. Applications of AJM process

Among various abrasive machining technologies, AJM process is having several recent and future application possibilities (Haldar et al., 2018) like,

Johnson, 1950	Welding, laser cladding, painting
Griffiths et al., 1997	Substrate surface preparation for plasma spray coatings
Balasubramaniam et al., 1999	Independent of surface profile, deburring

Wakuda et al., 2002	Clarification of erosive wear mechanism of a material, and, micromachining
Chauhan et al., 2010	
Jain et al., 2014	
Liu et al., 2008	Abrasive polishing
Ke et al., 2011	Hard surface cleaning, finishing
Tyagi, 1012	Machining of brittle and ductile materials; impingement angle of 90° for brittle materials and 20-30° for ductile material
Li et al., 2017	Surface modification (like hardening) by shot-peening
Liu et al., 2019	Rust cleaning

In recent years, several investigations are reported to improve the quality of abrasive jet machined components, optimization of process variables (Muju & Pathak, 1988), and control issues of health hazards.

1.2. Applications and AJM of ceramic alumina

The demand for machining superior quality ceramic alumina (Al_2O_3) is gradually increasing for its various progressive applications in tool inserts, drawing tools, corrosion and wear protection linings, friction discs, armor flats, ballistic protection components, electrical insulators, cryogenic isolators, heat sinks, ceramic seals (Chang & Kuo, 2007; Chak & Rao, 2007), etc. due to its cost benefit ratio as compared to other advanced ceramics featuring high hardness, high strength, high refractoriness stiffness, high modulus of elasticity (Silva et al., 2014), etc. Alumina is used for biomedical implants like hip and knee joints (Zeng, 2008). For its excellent corrosion-resistant ability even at an elevated temperature (Auerkari, 1996), is suitable for applications in chemical industries. Unique electronic characteristics of alumina find applications to make next generation computer memory and piezo-ceramic sensors (Pawar et al., 2015). Alumina is well known for its difficult-to-machine characteristics as it has high hardness and refractoriness along with some other excellent mechanical properties. And in these cases, AJM is found to be quite effective (Jain et al., 2002) for drilling, cutting, slotting, surface preparation, etc. in alumina.

Alumina composite was observed (Wakuda et al., 2003) to have produced a rougher surface with higher MRR using synthetic diamond than silicon carbide by utilizing their micro-abrasive jets. AWJM of alumina ceramics by oscillating the water abrasive jet nozzle was investigated Xu & Wang, (2006) to report a significant increase (as much as 82%) in the depth of cut. Different works in AJM process related to MRR, kerf, surface roughness, depth of cut achieved and taper angle made were also reported (Srikanth et al., 2014).

1.3. Present status of AJM performance analysis using RSM and ANN

A research group developed (Karmakar et al., 2020; Ghara, 2018), an indigenous AJM system with the facility of precise variation and control of abrasive flow rate and abrasive and carrier gas (air) mixing ratio, and investigated on abrasive jet machining of soda-lime glass as well as porcelain tiles employing common silica sand and SiC abrasives, and surface preparation of stainless steel specimens by varying AJM process parameters. They reported higher material removal ability of SiC abrasives than silica sand.

Regression technique along with response surface methodology (RSM) became a useful mathematical modeling for process parameters optimization of welding (Kavitha et al., 2021), machining processes (Xu & Wang, 2006), like processes, however, complex relationships would be difficult to model with this, and artificial neural networks (ANN) would be a good choice in such cases. Abrasive jet drilling of glass was attempted (Samani et al., 2014) to develop a precise predictive model by using various ANN architectures which were determined by calculating variance between actual experiment results and predicted results, and various errors. An experiment-based work on AJM of glass was reported (Abdalla et al., 2016), to find out the relative influence of different process variables. They used ANN to model MRR precisely and found only about 5% estimation error.

In this investigation, the influence of input AJM process parameters to obtain maximum MRR and low associated nozzle wear on the 4 mm thick alumina flat using SiC abrasive, are explored in an indigenously designed AJM setup. The ANN has been used to make a prediction model of the AJM process.

2. Experimental Investigation on Drilling Blind Holes in Alumina Flat

2.1. Materials and method

The indigenously developed abrasive jet setup capable of controlling the abrasive flow rate and abrasive mixing ratio that is used in this work is shown in Fig. 1. A sample hole machined on an alumina A99 flat workpiece and a typical application of taper hole machined by abrasive jet erosion are shown in Fig. 2 (a) and (b) respectively.

The experiment is carried out for machining crater on the 4 mm uniform alumina A99 flat work pieces. Table 1 shows the constituents of the work piece used. Among three types of commercial alumina (Silva et al., 2014), that are used for armor applications, A99 alumina is reported least relative density of 97.1 and maximum hardness of 14.8±0.7 HV, and bending strength of 227±20 MPa with Weibull modulus of 8.

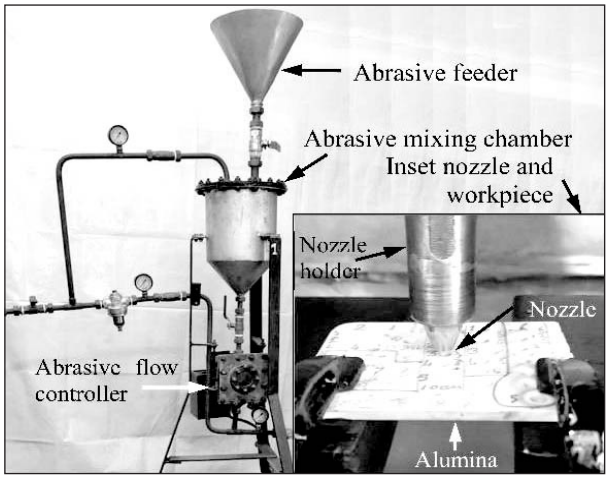

Fig. 1. Indigenously developed AJM setup with inset nozzle and workpiece.

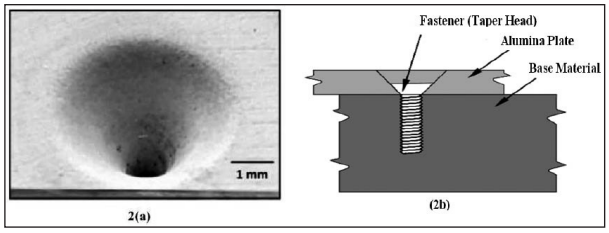

Fig. 2. (a) A hole machined on a 4 mm thick alumina A99 workpiece by using SiC abrasive jet (b) possible application of drilled alumina flat.

Experiments are designed as per response surface methodology (RSM) matrix corresponding to 3-factor 3-level system. In experiment set I and set II, three SOD values were chosen evenly within 2 to 4 mm, and abrasive grain size was similarly taken within 100 to 200 µm, while the abrasive flow rate of three values was evenly taken within 110 to 120 $g.min^{-1}$ for experiment set I, and 120 to 140 $g.min^{-1}$ abrasive flow rate for experiment Set II. Air pressure is kept constant as 4 $kgf.cm^{-2}$ and 6 $kgf.cm^{-2}$ during experiment set I and experiment set II respectively. The detail of calibration at 6 $kgf.cm^{-2}$ air pressure and some analyses done are similar to that detailed in (Ghara et al., 2018). The stainless steel nozzle of 2 mm outlet diameter is used to form an abrasive jet. Instead of a through hole, the blind cavity is formed in the alumina workpiece within the 20s of machining time. MRR and nozzle wear rate (NWR) are found out by the difference in weight of work sample and nozzle before and after the experimental runs. Box-Behnken design of RSM is used to choose experimental runs which are tabulated in Table 2.

2.2. Modeling abrasive jet drilling using ANN

A back-propagation type ANN with Levenberg-Marquardt training method is constructed by using obtained data (Table 2) during making blind holes employing an abrasive jet to estimate MRR and NWR. The number of hidden layer in ANN architecture has been taken one because the sample data are less complex and with fewer dimension. Different architectures of ANN with varying hidden nodes and layers are tried employing Minitab R2017a software to get the ANN structure giving minimum estimation error. Seletion of the number of neurons in the hidden layer has been performed and is detailed in the results and discussion section. The minimum error giving network is evaluated to have four input nodes (representing pressure, grain size, SOD, and abrasive flow rate), twenty nodes in the only one hidden layer, and two output nodes (representing MRR and NWR). It is denoted by 4-20-2 architecture (Fig. 3). Training is stopped when the mean square error value stops reducing with the number of iterations.

Table 1
Chemical composition (wt %) of commercial alumina A99.

Composition	Al_2O_3	SiO_2	CaO	MgO	Na_2O	Fe_2O_3
wt.%	99.7	0.0	0.0	0.1	0.1	0.02

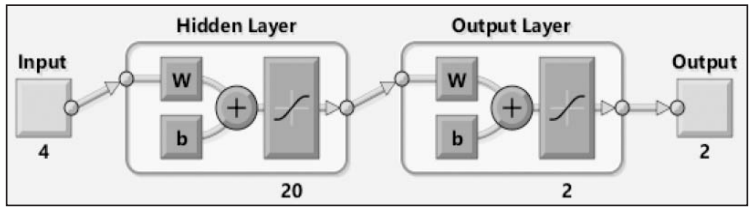

Fig. 3. 4-20-2 structure of ANN used.

Table 2
MRR and nozzle wear rate of SS nozzle during AJM of alumina A99 flat.

Run order	Air pressure ($kgf.cm^{-2}$)	Grain size (µm)	SOD (mm)	Abrasive flow rate ($g.min^{-1}$)	Machining time (s)	MRR ($g.min^{-1}$)	NWR ($g.min^{-1}$)
1	6	150	4	120	19.97	0.142900	0.006818
2	6	150	3	130	20.11	0.142700	0.006130
3	6	100	3	120	20.58	0.070810	0.002636
4	6	200	4	130	20.80	0.099950	0.001636
5	6	150	3	130	20.25	0.142100	0.006136
6	6	150	2	140	20.48	0.098200	0.002636
7	6	150	2	120	20.69	0.104270	0.006954
8	6	150	4	140	20.22	0.068310	0.005363
9	6	100	2	130	20.40	0.076180	0.001000
10	6	200	3	140	20.43	0.092000	0.002636
11	6	100	3	140	20.85	0.072136	0.002220
12	6	100	4	130	20.33	0.098510	0.004000
13	6	200	3	120	20.43	0.088000	0.004500
14	6	150	3	130	20.45	0.142500	0.006101
15	6	200	2	130	20.58	0.091954	0.006500
16	4	200	4	115	20.41	0.084500	0.002630
17	4	150	3	115	20.19	0.120004	0.008400
18	4	100	2	115	20.47	0.070590	0.002636
19	4	150	2	110	20.27	0.142770	0.002500
20	4	150	2	120	20.43	0.065000	0.002590
21	4	100	3	110	20.53	0.080530	0.001318
22	4	200	2	115	20.8	0.076000	0.002220
23	4	100	3	120	20.52	0.075900	0.002220
24	4	200	3	120	20.29	0.080460	0.001310
25	4	150	4	120	20.82	0.097200	0.003181
26	4	150	4	110	20.86	0.088500	0.000450
27	4	100	4	115	20.68	0.0883604	0.002636
28	4	150	3	115	20.53	0.132500	0.008000
29	4	150	3	115	20.52	0.134180	0.008220
30	4	200	3	110	20.05	0.125100	0.002270

3. Results and Discussion on the Present Work

Observations made in experiment sets I and II are first analyzed through ANOVA separately. Surface and contour plots are also made to find out the parametric influence on the response. Then with all the data of both the experiment sets, ANN is constructed for estimation.

3.1. Experiment set I performed at 4 kgf.cm^{-2} air pressure

Experiment set I is performed by setting 4 kgf.cm^{-2} system pressure. Analysis of variance (ANOVA) is done by adopting 95% confidence level to evaluate relative contribution of each variable on AJM performance using Minitab 17 software. Results obtained related to MRR are shown in Table 3. The small *p*-value of 0.019 for mass flow rate (Q), a value 0.016 for the interaction of SOD, a value of 0.006 for a square of grain size, d and a value of 0.023 for the square of SOD, δ indicate good correlation of them with MRR. 92.18% is the value of correlation coefficient, R^2 for MRR that is more than 90%, thereby validating the model and it can be stated that parameters are significant. The low *p*-value (0.026) of the model also supports this.

Optimal values of material removal rate can be obtained through Fig. 4(a,b) and are given in Table 4. Fig.s 4(a, b) shows the influence of abrasive particle size and SOD on workpiece MRR with a set 115 g/min flow rate. MRR rises slowly

Table 3
ANOVA for MRR under 4 kgf.cm^{-2} air pressure.

Source	DOF	Adj sum of squares	Adj mean of squares	F-value	p-value
Model	9	0008764	0.000974	6.55	0.026
Linear	3	0.002075	0.000692	4.65	0.065
d	1	0.000320	0.000320	2.16	0.202
δ	1	0.000002	0.000002	0.01	0.908
Q	1	0.001752	0.001752	11.79	0.019
Square	3	0.004399	0.001466	9.87	0.015
d*d	1	0.002987	0.002987	20.10	0.006
δ*δ	1	0.001565	0.001565	10.53	0.023
Q*Q	1	0.000365	0.000365	2.45	0.178
Two-way interaction	3	0.002290	0.000763	5.14	0.055
d* δ	1	0.000021	0.000021	0.14	0.719
d*Q	1	0.000399	0.000399	2.68	0.162
δ*Q	1	0.001869	0.001869	12.58	0.016
Error	5	0.000743	0.000149		
Lack-of-fit	3	0.000623	0.000208	3.46	0.232
Pure error	2	0.000120	0.000060		
Total	14	0.009507			
[d = Size of abrasive grain, Q = Mass abrasive flow rate and δ = SOD]					

Table 4
Summary of optimized MRR at a set 4 kgf.cm^{-2} system pressure.

SOD (mm)	Grain size (μm)	Avrasive flow rate (g.min^{-1})	MRR (g.min^{-1})
2.4 to 3.6	130 to 175	115 (constant)	> 0.12
3 (constant)	145 to 185	107 to 114	> 0.13
1.5 to 3.2	150 (constant)	107 to 114	> 0.13

as grain size is incremented, reaches a maximum in a range of 130 to 175 µm and after that, it goes on decreasing. It is likely due to bigger abrasive particles causing increasingly larger shock load onto the workpiece to the point of maxima, but the further increment in particle cross-section may cause less impact thereby reducing MRR. It is also noted that MRR slowly rises with increasing SOD and gains a maximum near to 2.4 to 3.6 mm and after that, it decreases with increasing SOD. Initially, just after departing the nozzle, the abrasive particle moves with acceleration and then attains a uniform velocity, and then decelerates similar to a gun departed bullet (projectile) trajectory though it happens in AJM in a micro-range as with that compared. Naturally, the particles attain higher MRR due to impacts when the particle velocity is maximum in its trajectory. So, the optimum value of SOD might be influenced by abrasive jet pressure. At higher pressure, higher SOD may result in higher MRR.

Surface and contour plots in Fig. 5 (a, b) show the effect of size of abrasive particles and abrasive flow rate on MRR by setting 3 mm SOD (fixed). MRR is higher when the grain size is within 140 to 185 µm and decrease beyond the range. It is probably because initially, MRR increases with larger grain size and when further bigger grains are used above a certain value, it causes decrease of jet flow velocity that results in reduction of MRR. The abrasive flow rate of 107 to 114 g/min with more than 145 to 180 µm grain size of abrasives attains higher MRR. Even, MRR decreases at a low rate while the abrasive flow rate increases further due to a higher number of particles may collide among themselves thereby losing energy.

Fig. 6 (a, b) depicts change of MRR with varying flow rate and SOD with 150 µm grain size. MRR is high within 1.5 to 3.2 mm of SOD with a 107 to 114 g.min^{-1} abrasive flow rate. Out of that specified region, MRR is found to gradually decrease. Up to a certain limit of SOD, grains accelerate thereby gaining kinetic energy and increasing MRR, but when SOD is further increased, the particle velocity reduced and the jet also get diverged, that results in decreasing of MRR.

Nozzle wear rate (NWR) in the experiment at 4 kgf.cm^{-2} air pressure is measured and shown in Table 2. Analysis of variance is done and results of NWR are shown in Table 5 with 95% confidence level. A statistical characteristic, *p*-value has been calculated for each term and is summarized in Table 5.

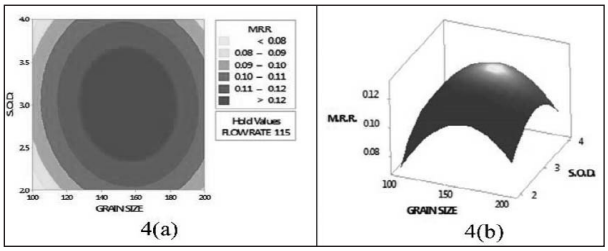

Fig. 4. (a) Contour plot, and (b) surface plot showing a variation of MRR related to SOD (mm) and grain size (µm) at a constant flow rate.

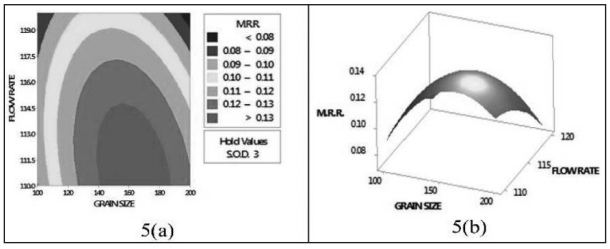

Fig. 5. (a) Contour plot, and (b) surface plot showing a variation of MRR related to abrasive flow rate (g.min^{-1}) and grain size (µm) at a constant SOD.

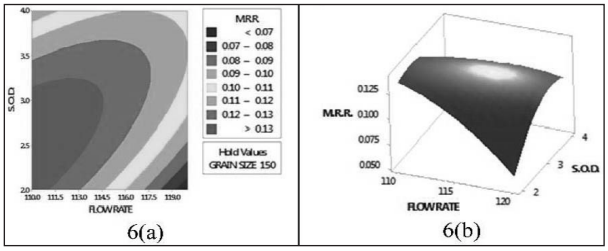

Fig. 6. (a) Contour plot, and (b) surface plot showing a variation of MRR related to SOD (mm) and abrasive flow rate (g.min^{-1}) at a constant grain size.

Less value of *p* (0.066) of interaction of SOD and Q, 0.000 value of square of size of abrasive particles, SOD and Q show that they have quite good correlations with the response, that is, nozzle wear. The correlation coefficient R^2 for NWR is as high as 98.32% indicating the model is quite significant, as also found out through a small model *p*-value of 0.001. Other parameters such as grain size (d), two-way interaction (d*δ), and SOD (δ) are somewhat less significant. Fig. 7(a,b) shows graphical presentations of wearing of nozzle related to the sizes of abrasive and SOD in the form of contour plot and surface plot respectively maintaining flow rate Q of 115 g.min^{-1}. NWR attains a maximum at the region of 140 to 160 µm grain sizes and 2.80 to 3.20 mm SOD. The nozzle wear might be increased due to the interaction of bigger sharp edges of bigger grits, but beyond a certain grain size, the contact area between particle and nozzle wall may decrease which may have reduced NWR.

Table 5
ANOVA for nozzle wear under 4 kgf.cm^{-2} air pressure.

Source	DOF	Adj sum of squares	Adj mean of squares	F -value	p-value
Model	9	0.000093	0.000010	32.54	0.001
Linear	3	0000001	0.000000	1.17	0.408
d	1	0.000000	0.000000	0.06	0.821
δ	1	0.000000	0.000000	0.44	0.539
Q	1	0.000001	0.000001	3.02	0.143
Square	3	0.000089	0.000030	93.66	0.000
d*d	1	0.000034	0.000034	107.88	0.000
δ*δ	1	0.000026	0.000026	81.30	0.000
*Q** *Q*	1	0.000042	0.000042	134.19	0.000
2-way interaction	3	0.000003	0.000001	2.80	0.148
d* δ	1	0.000000	0.000000	0.13	0.730
d * *Q*	1	0.000001	0.000001	2.74	0.159
δ* *Q*	1	0.000002	0.000002	5.52	0.066
Error	5	0.000002	0.000000		
Lack-of-fit	3	0.000001	0.000000	12.46	0.075
Pure error	2	0.000000	0.000000		
Total	14	0.000094			
[d= Grain size, Q= Mass flow rate, and δ= SOD]					

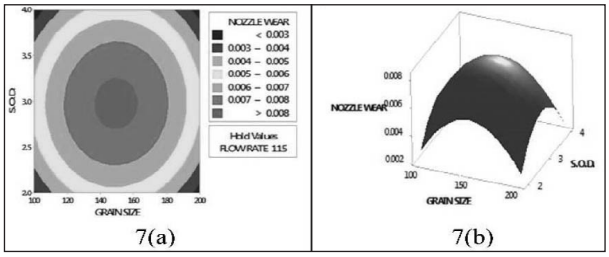

Fig. 7. (a) Contour plot, and (b) surface plot showing NWR related to SOD (mm) and grain size (µm) at a constant flow rate.

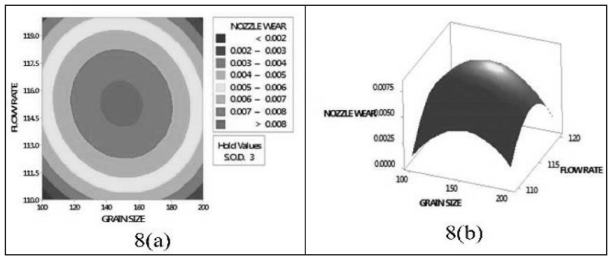

Fig. 8. (a) Contour plot, and (b) surface plot showing NWR related to abrasive flow rate (g.min^{-1}) and grain size (µm) at a constant SOD.

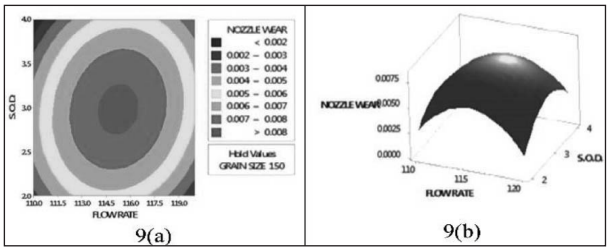

Fig. 9. (a) Contour plot, and (b) surface plot showing NWR related to SOD (mm) and abrasive flow rate (g.min^{-1}) at a constant grain size.

In Fig. 8 (a, b), change in nozzle wearing with rising grain sizes and flow rates are indicated as a contour plot and a surface plot where SOD is kept constant at 3 mm. The contour and surface plots show that NWR is higher between grain sizes of 130 to 160 µm at abrasive flow rate of 114 to 116.5 g.min^{-1}. NWR increases with the bigger grains up to a certain limit and a further increase of both flow rate Q and grain size may reduce contact time and contact area of grits with nozzle wall, thus reducing nozzle wearing.

Similar to above, Fig. 9(a, b) represent change of weight loss pattern at different values of Q and SOD at 150 µm grits. The maximum weight loss of nozzle takes place between flow rate of 114 to 116.5 g.min^{-1} at SOD of 2.8 to 3.20 mm as observed from these plots. Nozzle wearing is detected at around the four corners of contour and surface plots corresponding to any combination that support the previous explanations. Summary of optimized values are given in Table 6.

The maximum MRR takes place using 150 µm SiC particles which are effective with the set system pressure. The higher irregular shapes of abrasives indicate sharp edges which might be the reason for effective material removal in this case.

3.2. Experiment set II performed at 6 kgf.cm^{-2} air pressure

Similarly, experiment set II was conducted at 6 kgf.cm^{-2} air pressure following 3-factor 3-level RSM matrix. Similar analyses were done and contour and surface plots of MRR concerning process parameters and their interactions were prepared as detailed elsewhere (Adak et al., 2021). Table 7 summarizes the optimal results thus obtained. The range of the process parameters and corresponding high MRR exceeding 0.14 g/min can easily be observed.

Weight loss of nozzle indicating nozzle wearing was computed along with MRR and ANOVA was also done. Details of these results are available in reference (Adak et al., 2021). Optimized values are extracted from (Adak et al., 2021), and are tabulated in Table 8.

3.3. Summary of results obtained from experiment set I and II for low NWR and high MRR

Optimized results as obtained from Experiment Set I and II through ANOVA are summarized in Table 9 corresponding to low NWR at high MRR. Abrasive of a low range of grain size is good as concerned with surface finish, somewhat low abrasive flow rate gives high MRR and low nozzle wearing, high range of SOD is favorable for low NWR as bouncing and striking of abrasives to nozzle becomes less. From experiment set I and II results, it is observed that MRR rises and NWR decrease with increasing carrier gas pressure. Higher gas pressure produces higher jet velocity which might float and suspend the abrasives well

Table 6
Summary of optimized NWR at 4 kgf.cm^{-2} air pressure

SOD (mm)	Abrasive grain size (µm)	Abrasive flow rate (g.min^{-1})	NWR (g.min^{-1})
2.80 to 3.20	140 to 160	115 (constant)	>0.008
3 (constant)	135 to 160	114 to 116.5	>0.008
2.80 to 3.20	150 (constant)	114 to 116.5	>0.008

Table 7
Summary of optimized MRR with 6 kgf.cm^{-2} system pressure.

SOD (mm)	Abrasive grain size (µm)	Abrasive flow rate (g.min^{-1})	MRR (g.min^{-1})
2.7 to 3.6	140 to 160	130 (constant)	>0.14
3 (constant)	140 to 165	125 to 130	>0.14
2.75 to 4	150 (constant)	123 to 131	>0.14

Table 8
Summary of optimized NWR values at 6 kgf.cm^{-2} air pressure.

SOD (mm)	Abrasive grain size (µm)	Abrasive flow rate (g.min^{-1})	NWR (g.min^{-1})
2 to 4	140 to 160	130 (constant)	>0.006
3 (constant)	140 to 180	<130	>0.006
<2	150 (constant)	< 120	>0.007

Table 9
The possible set of input for which the output will be optimum.

System pressure (kgf.cm^{-2})	Abrasive grain size (µm)	Abrasive flow rate (g.min^{-1})	SOD (mm)	MRR (g.min^{-1})	NWR (g.min^{-1})
4	170	110	2	0.1445	0.0019
6	160	125	3	0.168	0.0095

Table 10
Variation of performance results, training state results and regression results of neural network training with the variation in number of neurons in the hidden layer.

No of neuron	Variation of the result of neural network training									
	Performace Result				Training state Result		Regression Result (R)			
	Validation		Best Validation		Gradient (10^{-5})	Mu (10^{-7})	Training	Validation	Test	All
	Iteration	Epoch	MSE (10^{-5})	Epoch						
5	10	10	11.807	4	58.12	10	0.942	0.995	0.967	0.947
10	13	13	9.5227	7	5.52	1	0.971	0.987	0.955	0.969
15	10	10	37.8	4	0.20	1	0.983	0.917	0.972	0.973
20	15	15	8.616	9	0.03	0.0001	0.999	0.986	0.927	0.988
30	10	10	58.56	4	0.78	0.000001	0.996	0.949	0.963	0.976
50	8	8	38.25	2	0.35	0.001	0.986	0.941	0.919	0.968

Table 11
Trained value and experimental results of MRR and NWR.

Pressure ($kgf.cm^{-2}$)	Grain size (μm)	SOD. (mm)	Abrasive flow rate ($g.min^{-1}$)	MRR ($g.min^{-1}$)		NWR ($g.min^{-1}$)	
				Predicted value	Experimental value	Predicted value	Experimental value
6	200	2	130	0.0920	0.0919	0.0071	0.0065
4	200	3	110	0.1248	0.1251	0.0023	0.00227

and result in lower NWR inside the nozzle and higher MRR.

3.4. Discussion on results obtained through the application of ANN

Among 28 experimental datasets from Table 2, for training, validation, and testing purpose, 70%, 15%, and 15% of data are selected respectively as a standard procedure. The performance results, training state results and regression results of neural network training have been done with the variation in number of neurons, or nodes, in the hidden layer. The number of neuron in the hidden layer has been selected with the highest value of R in the regression results and the lowest value of MSE in the performance results of neural network training. The value of each results has been reflected in Table 10 which shows that best performance has been obtained with 20 number of neurons in the hidden layer. So, further study has been done with 20 number of neurons in the hidden layer and the corresponding neural network architecture is 4-20-2.

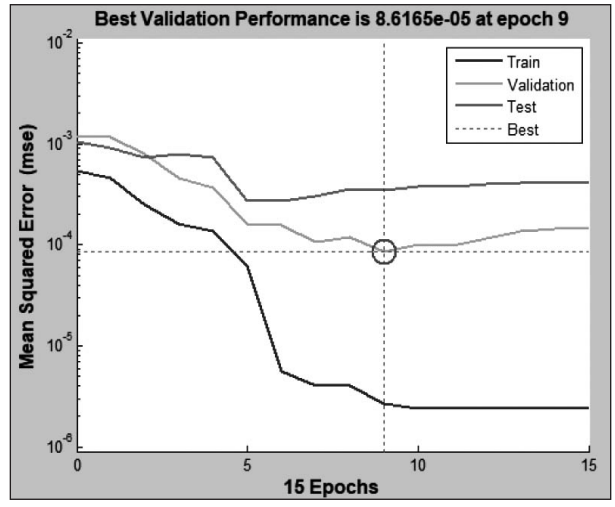

Fig. 10. Validation performance.

After training the network eight times, it is detected that the mean square error value becomes close to 0, and the coefficient of determination (R) becomes almost 1 which is quite satisfactory. After completing the training stage with the Leverberg-Marquardt training algorithm, validation is completed with 15 iterations. Fig. 10 depicts that the validation

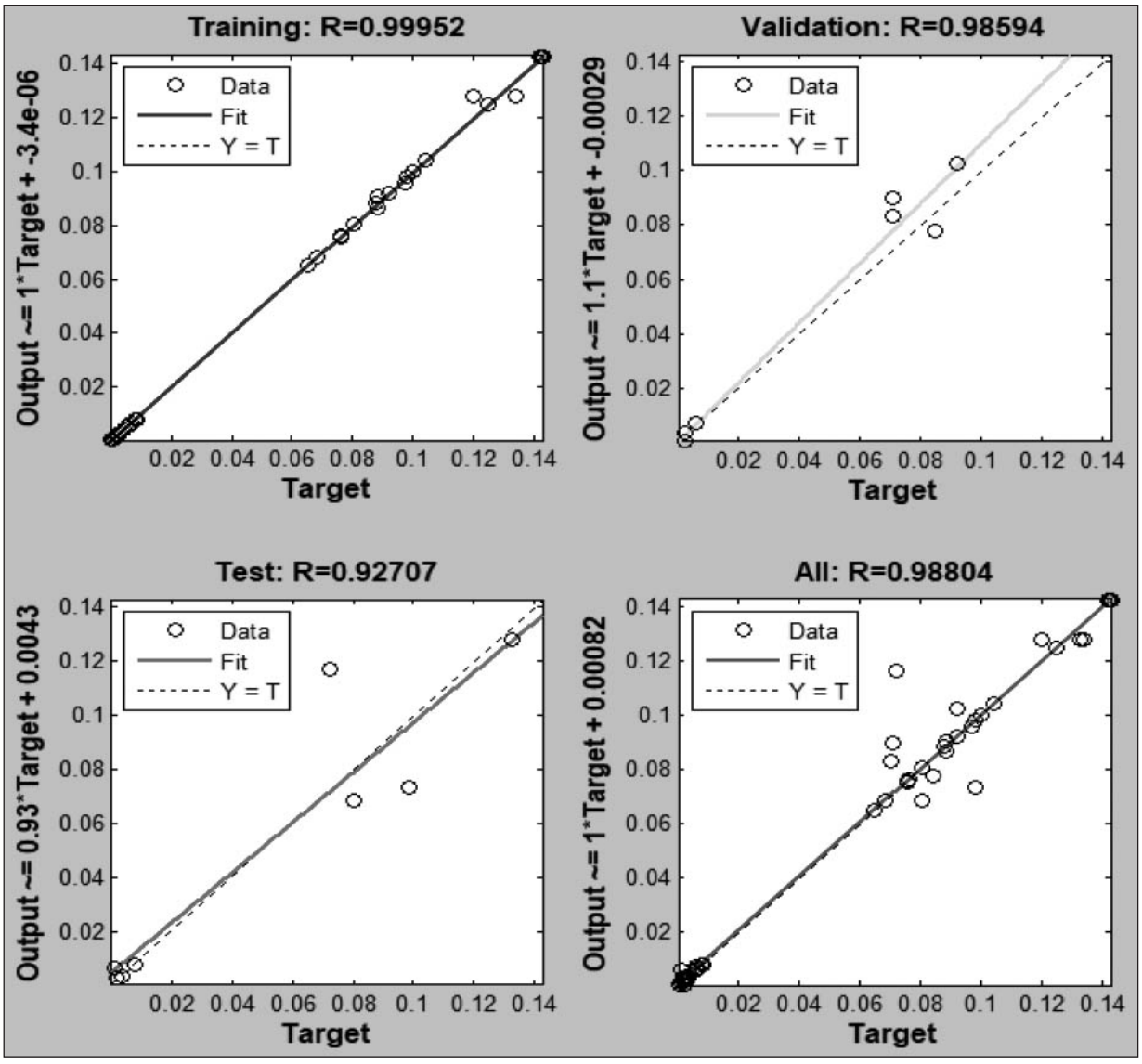

Fig. 11. Comparisons between target and output of ANN.

performance rate is satisfying within 15 epoch points and the best validation is obtained to be 0.000086 at 9 epoch points. In this figure, the MSE value of testing performance is less than the MSE of validation because proper training has likely been done with the sample data.

Experimental results are compared with the ANN model proposed in Fig. 11. Solid lines represent regression fitting between targets and outputs for training, validation, and testing. R-values for training, validation and testing appear to be 0.999, 0.986 and 0.927 respectively. The overall analysis gives the R-value of 0.988. In this case, R = 1 means perfect matching between the experimental value (target) and ANN output. Since, ANN cannot usually be made to learn perfectly, therefore, if R is close to 1, it may be considered quite acceptable, and the neural network becomes the better one. So, R-values are found quite satisfactory in the present case. In Fig.s 12(a) and 12(b), comparisons between the experimentally obtained values and ANN output values are shown.

Based on a strong training algorithmic tool, the ANN model can predict MRR value for a subsequent experimental run well before. It has been observed in Fig. 12(a) that the range of variation between run orders reduces towards the mean value for MRR indicating close matching of the predicted values with that of the experimental observations. In case of nozzle wear also, predicted values for nozzle wear rate show good matching with the experimental values as shown in Fig. 12(b) except for few deviations in some experimental runs such as in experiment No. 11, 17 and 23.

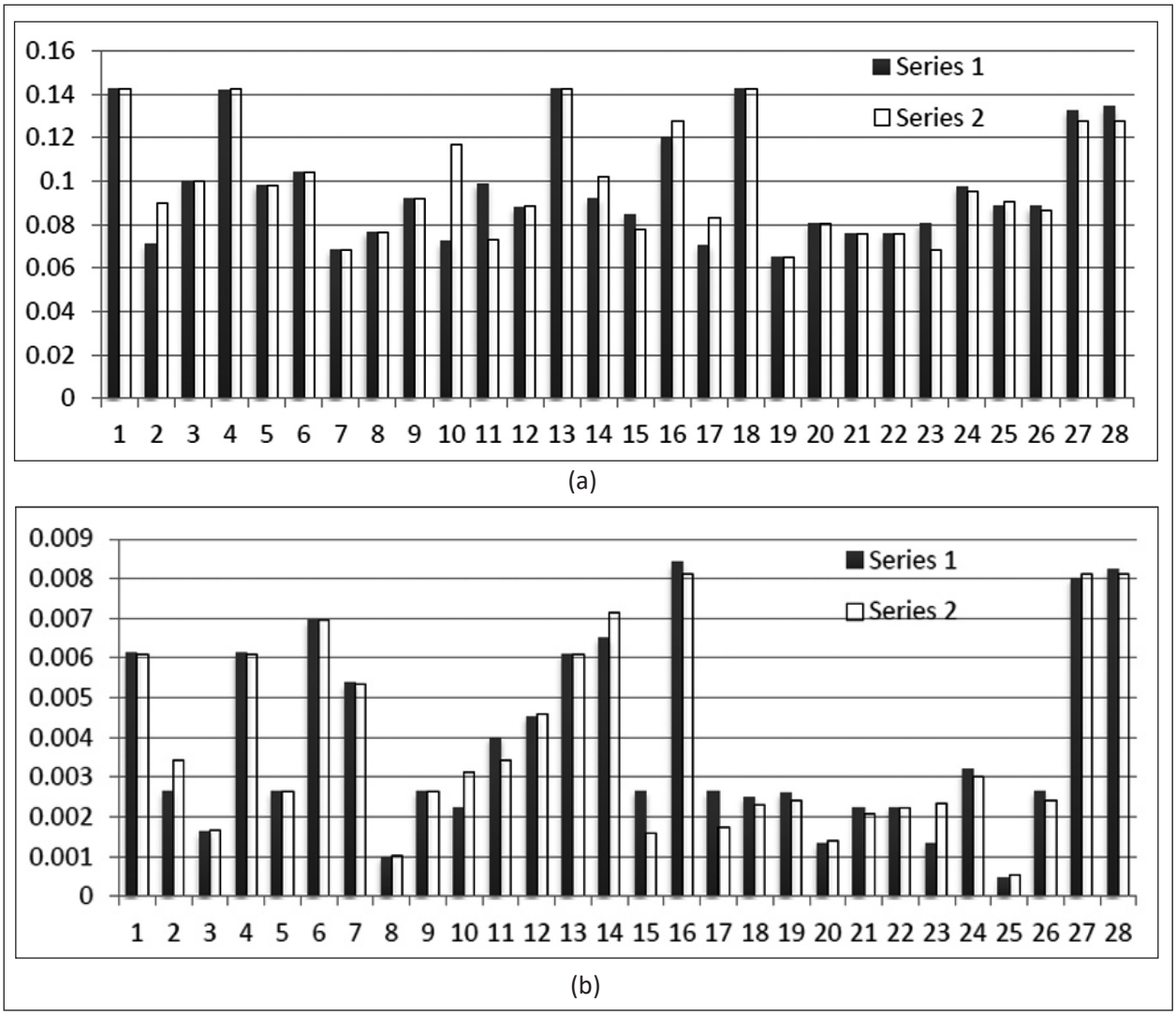

(Series1: Experimental, Series 2: ANN Predicted)

Fig. 12. Experimental and predicted values of (a) MRR, and (b) NWR at different experimental runs.

Finally, the authors have compared in Table 11 the experimental value of MRR and NWR of run orders 15 and 30 in Table 2 with the ANN outcome when the input of the same run order is given to the model. The differences between trained values and experimented values are remarkably less and quite satisfactory. ANN is, therefore, found to be a quite effective tool for prediction or estimation for MRR and NWR in AJM.

4. Conclusion

Following are the conclusions that may be made out of the work done.

- SiC abrasive jet is effective for material removal in drilling on alumina ceramic tiles.
- At a constant flow rate of an air-abrasive mixture, MRR and nozzle wear rate increase with the size of abrasive grains up to a value and then gets lowered.
- From experimental data, it is revealed that both MRR and nozzle wearing have an increasing trend related to the rate of flow of abrasive particles.
- Within the range of the current experiment, MRR has an increasing tendency while there is a decreasing tendency of nozzle wearing when system pressure is set higher.
- The artificial neural networks model with a 4-20-2 configuration is found to be suitable, fast, and reliable based on the least MSE and favourable R values.
- Artificial neural network shows its effectiveness in estimating MRR having a quite close correlation with the actual performance. The differences between trained values and

experimented values are considerably less in case of MRR and satisfactory.

- For estimating nozzle wear rate, ANN estimates often show considerable deviations. If the number of experimental runs is increased, ANN estimation is expected to be better.

Acknowledgements

The authors are thankful to Kalyani Government Engineering College, Kalyani, India for providing all sorts of support needed for carrying out the experimental investigation.

References

Abdalla, H.S., Elkaseer, A., & Nassef, A. (2016). Abrasive jet machining of glass: Experimental investigation with artificial neural network modelling and genetic algorithm optimisation. *Cogent Engineering*, *3*, 1-18.

Adak, D.K., Dutta, P., Das, S., & Haldar, B. (2021). Machining alumina plates using abrasive jet of silicon carbide. *IOP* Conference Series: Materials Science and Engineering, *1080,* 012020.

Auerkari, P. (1996). *Mechanical and Physical Properties of Engineering Alumina Ceramics*. VTT Technical Research Centre of Finland.

Aydin, G., Karakurt, I., & Aydiner, K. (2011). An investigation on surface roughness of granite machined by abrasive waterjet. *Bulletin of Materials Science, 34*, 985-992.

Balasubramaniam, R., Krishnan, J., & Ramakrishnan, N. (1999). An experimental study on the abrasive jet deburring of cross-drilled holes. International *Journal of Material Processing Technology*, 178-182.

Chak, S.K., & Rao, P.V. (2007). Trepanning of Al_2O_3 by electro-chemical discharge machining (ECDM) process using abrasive electrode with pulsed DC supply. *International Journal of Machine Tools and Manufacture, 47*, 2061-2070.

Chang, C.W., & Kuo, C.P. (2007). An investigation of laser-assisted machining of Al_2O_3 ceramics planing.*International Journal of Machine Tools and Manufacture, 47*, 452-461.

Chauhan, A.K., Goel, D.B., & Prakash, S. (2008) Erosion behaviour of hydro turbine steels. *Bulletin of Materials Science, 31*, 115-120.

Chauhan, A.K., Goel, D.B., & Prakash, S. (2010). Erosive wear of a surface coated hydroturbine steel. *Bulletin of Materials Science*, *33*, 483-489.

Ghara, T., Desta, G., Das, S., & Haldar, B. (2018). Abrasive jet machining: drilling of porcelain tiles and soda lime glass. In: Davim PSJP (ed) *Advances in Materials, Mechanical and Industrial Engineering.* Springer. 189-208.

Griffiths, B. J., Gawne, D. T., & Dong, G. (1997). The role of grit blasting in the production of high-adhesion plasma sprayed alumina coatings. *Proceedings of the Institution of Mechanical Engineers, Part B: Journal of Engineering Manufacture, 211*, 1-9.

Haldar, B., Ghara, T., Ansari, R., Das, S., & Saha, P. (2018). Abrasive jet system and its various applications in abrasive jet machining, erosion testing, shot-peening, and fast cleaning. *Materials Today: Proceedings, 5*, 13061-13068.

Inasaki, I., Tönshoff, H. K., & Howes, T. D. (1993). Abrasive machining in the future. *CIRP Annals - Manufacturing Technology*, *42,* 723-732.

Jain, V. K., Choudhury, S. K., & Ramesh, K. M. (2002). On the machining of alumina and glass. *International Journal of Machine Tools and Manufacture, 42,* 1269-1276.

Jain, V. K., Sidpara, A., Balasubramaniam, R., & Lodha, G. (2014). Micromanufacturing: a review-part I. *Proceedings of the Institution of Mechanical Engineers, Part B: Journal of Engineering Manufacture, 228,* 973-994.

Johnson, W. A. (1950). The Engineering implications and Economics of surface preparation of mild steel prior to fabrication. *Proceedings of the Institution of Mechanical Engineers, 162,* 49-65.

Kalpakjian, S., & Schmid, S. R. (2007). *Manufacturing Engineering and Technology*. 4th. Pearson Education.

Karmakar, A., Ghosh, D., Adak, D. K., Mandal, B., Das, S., Ahmed, M., & Haldar, B. (2020). Abrasive jet machining of soda lime glass and laminated glass using silica sand. In: Kanthababu MSSM (ed) *Advances in Unconventional Machining and Composites*. Springer, 163-178.

Kavitha, M., Manickavasagam, V. M., Sathish, T., Gugulothu, B., Satihish Kumar, A., Karthikeyan S., & Subbiah R. (2021). Parameters optimization of dissimilar friction stir welding for AA7079 and AA8050 through RSM. *Advances in Materials Science and Engineering,* Epub ahead of print.

Ke, J. H., Tsai, F. C., Hung, J. C,. Yang, T. Y., & Yan, B. H. (2011). Scrap wafer regeneration by precise abrasive jet machining with novel composite abrasive for design of experiments. *Proceedings of the Institution of Mechanical Engineers,*

Part B: Journal of Engineering Manufacture, 225, 881-890.

Li, K., Zheng, Q., Li, C., Shao, B., Guo, D., Chen, D., Sun, J., Dong, J., Cao, P., & Shin, K. (2017). Characterization of surface modification of 347 stainless steel upon shot peening. *Scanning.* Epub ahead of print 2017.

Linken, B. S. (2015). A review on properties of abrasive grits and grit selection. *International Journal of Abrasive Technology, 7,* 46-58.

Liu, H., Wang, J., & Huang, C. Z. (2008). Abrasive liquid jet as a flexible polishing tool. *International Journal of Materials and Product Technology, 31,* 2-13.

Liu, Y., Zhang, H., Ranjith, P. G., Jianping, W., & Liu, X. (2019). Wear mechanism of abrasive gas jet erosion on a rock and the effect of abrasive hardness on it. *Geofluids.* Epub ahead of print 2019.

Mattison, A. M. (1964). The present and future of abrasive machining. *SAE International,* 837C, 1-8.

Melentiev, R., & Fang, F. (2018). Recent advances and challenges of abrasive jet machining. *CIRP Journal of Manufacturing Science and Technology, 22*, 1-20.

Muju, M. K., & Pathak, A. K. (1988). Abrasive jet machining of glass at low temperature. *Journal of Mechanical Working Technology, 17,* 325-332.

Pawar, P., Ballav, R., & Kumar, A. (2015). An overview of machining process of alumina and alumina ceramic composites. *Manufacturing Science and Technology, 3*(1): 10-15, 2015.

Samani, J. R., Beravala, H. S., Jadav, P. B., & Dusra, C. J. (2014). Artificial neural network modeling for prediction of performance in abrasive jet drilling process for glass material. *All India Manuf Technol Des Res Conf.,* 2201-2205.

Silva, M. V., Stainer, D., Al-Qureshi, H. A., Montedo, O. R. K., & Hotza, D. (2014). Alumina-based ceramics for armor application: mechanical characterization and ballistic testing. *Journal of Ceramics,* 1-6.

Srikanth, D. V., & Sreenivasa Rao, M. (2014). Metal removal and kerf analysis in abrasive jet drilling of glass sheets. *Procedia Mater Science, 6*, 1303-1311.

Tyagi, R. K. (2012). Abrasive jet machining by means of velocity shear instability in plasma. *Journal of Manufacturing Processes,* 14, 323-327.

Wakuda, M., Yamauchi, Y., & Kanzaki, S. (2002). Influence of micromachining on strength degradation of silicon nitride. *Proceedings of the Institution of Mechanical Engineers, Part B: Journal of Engineering Manufacture, 216,* 55-60.

Wakuda, M., Yamauchi, Y., & Kanzaki, S. (2003). Material response to particle impact during abrasive jet machining of alumina ceramics. *Journal of Materials Processing Technology, 132,* 177-183.

Xu, S., & Wang, J. (2006). A study of abrasive waterjet cutting of alumina ceramics with controlled nozzle oscillation. *The International Journal of Advanced Manufacturing Technology, 27,* 693-702.

Zeng, P. (2008). Biocompatible alumina ceramic for total hip replacements. *Materials Science and Technology, 24,* 505-516.

Deb Kumar Adak, M.E. (Production Engineering from Delhi College of Engineering) Assistant Professor, Mechanical Engineering Department, College of Engineering and Management, Kolaghat, W.B. since 12th March 2013. He is having 13 years of teaching experience from September 2009 and 20 years of industrial experience in Indian Air Force as Technical Supervisor from August 1989. Presently he is doing his Ph.D work on abrasive jet machining: a non-traditional machining process on harder material in Kalyani Govt. Engineering College, W.B. Presented papers in several International Conferences and also published papers on reputed Journals and Technical volumes etc.
(E-mail: debkumaradak1968@gmail.com)

Prosenjit Dutta obtained B.Tech in Mechanical Engineering from Techno India, Salt Lake in 2016, and M.Tech (Production Engineering) from Kalyani Govt. Engineering College, Kalyani in 2019. He is at present Pursuing Ph.D (Mechanical Engineering) at Indian Institute of Engineering Science and Technology since 2020. Broad domain of his research include Sintering and Processing of Engineering Ceramics.
(E-mail: prosenjitdutta.me@gmail.com)

Dr. Barun Haldar is Assistant Professor, Mechanical and Industrial Engg. Department, College of Engineering, Imam Mohammad Ibn Saud Islamic University (IMSIU), Riyadh, Saudi Arabia. He obtained Ph.D from IIT Kharagpur, India in 2016. He is specialized in Manufacturing Technology and his present research includes laser material processing, machining, non-traditional manufacturing, 3D printing in casting, etc.
(E-mail: dr.barun.haldar@gmail.com)

Dr. Santanu Das is Professor and ex-Head, Department of Mechanical Engineering, Kalyani Government Engineering College, Kalyani, West Bengal. He graduated and post graduated in Mechanical Engineering from Jadavpur University, Kolkata. He obtained Ph.D (Engineering) from IIT Kharagpur. He guided 11 Ph.D and 144 M.Tech theses, and 102 B.Tech projects in machining, grinding, welding, weld cladding, inventory management, MCDM applications, etc. He is guiding 06 Ph.D research scholars. He has 182 publications in Journals, 34 in Book Chapters, and 109 in International and 167 in National Conferences. He was awarded 'Shiksha Ratna' in 2018 by Government of West Bengal as an Outstanding Teacher. He delivered Engineer Soumitra Kumar De Memorial Lecture 2019 instituted by Kolkata Branch, The Indian Institute of Welding. He received Production Division Award and Second Prize of Railway Board 2019 from The Institution of Engineers (India) and one Best Paper award from Indian Institution of Industrial Engineering.

Dr. Naser Abdulrahman Alsaleh, Ph.D (University of Minnesota, Minneapolis, USA, 1999), Associate Professor, College of Engineering, Imam Mohammad Ibn Saud Islamic University (IMSIU), Riyadh, Saudi Arabia. He is specialized in Industrial Engineering and his research includes metal cutting, industrial automation, TQM, industrial safety, CAD/CAM, advanced manufacturing technology, etc.
(E-mail: naalsaleh@imamu.edu.sa)

Dr. Sibsankar Das Mahapatra has received B.Tech in Mechanical Engineering from Kalyani Govt Engineering College, Kalyani, India in 2007. He has obtained Masters and Ph.D in Mechanical Engineering from Jadavpur University. In 2016, he has joined as Assistant Professor in Mechanical Engineering Department, Kalyani Govt Engineering College, Kalyani. His research interests are on soft computing and real time control. (E-mail: sdmpmekgec@gmail.com)